Applied Catalysis A: General 467 (2013) 559–567

Contents lists available at ScienceDirect

Applied Catalysis A: General

journal homepage: www.elsevier.com/locate/apcata

The use of pulsed laser deposited seed layers for the aqueous solution growth of highly oriented ZnO nanowires on sapphire substrates at 95 °C: Study of their photocatalytic activity in terms of octadecanoic (stearic) acid degradation

G. Kenanakis[a,b,c,*], M. Pervolaraki[d], J. Giapintzakis[d], N. Katsarakis[a,b,c]

[a] Institute of Electronic Structure and Laser, Foundation for Research & Technology – Hellas, P.O. Box 1385, Vassilika Vouton, 711 10 Heraklion, Crete, Greece
[b] Center of Materials Technology and Photonics, School of Applied Technology, Technological Educational Institute of Crete, 710 04 Heraklion, Crete, Greece
[c] Science Department, School of Applied Technology, Technological Educational Institute of Crete, 710 04 Heraklion, Crete, Greece
[d] Nanotechnology Research Center and Department of Mechanical and Manufacturing Engineering, University of Cyprus, 75 Kallipoleos Avenue, P.O. Box 20537, 1678 Nicosia, Cyprus

ARTICLE INFO

Article history:
Received 11 March 2013
Received in revised form 19 July 2013
Accepted 20 July 2013
Available online xxx

Keywords:
Aqueous solution growth
Pulsed laser deposition
Seed layer
ZnO
Nanowires
Photocatalysis
Octadecanoic acid
Stearic acid

ABSTRACT

The photocatalytic activity of ZnO nanowires grown via an aqueous solution approach at 95 °C onto sapphire substrates, which were first pre-coated with ZnO seed layers deposited by pulsed laser deposition at various temperatures (400–700 °C), was investigated against the degradation of octadecanoic (stearic) acid under UV-A light illumination. The crystallinity of the ZnO seed layers, as well as their growth orientation along the *c*-axis, increases with deposition temperature. All chemically grown ZnO samples show narrower (0 0 2) reflections with significantly higher intensity than the seed layers deposited by pulsed laser deposition. The grain size, as well as the seed layer roughness, gradually increases with substrate deposition temperature. The nanowires' diameter also rises with seed layer's deposition temperature, ranging from ~40 ± 15 nm for 400 °C to ~155 ± 65 nm for 700 °C. The chemically grown ZnO nanowires exhibit relatively high transmittance values, especially those grown on sapphire substrates, which were pre-coated with seed layers deposited by pulsed laser deposition at 400 and 500 °C. All ZnO samples, including seed layers and nanowires' arrays, show very good photocatalytic activity regarding the degradation of octadecanoic (stearic) acid under UV-A light exposure. In specific, the photocatalytic activity of ZnO nanowires' arrays grown on top of a seed layer deposited by pulsed laser deposition at 600 °C is quite remarkable, showing the highest stearic acid disappearance rate, i.e., 4.22×10^{-8} mol/min (formal quantum efficiency = 4.48×10^{-3}) at 30 min of UV-A light illumination.

1. Introduction

Over the past two decades, various technologies have been developed in order to decompose environmental contaminants. Recently, there has been a considerable interest in the utilization of advanced oxidation processes (AOPs) for the complete destruction of complex organic pollutants, with a result in the formation of eco-friendly products [1–5]. The most widely known AOPs include heterogeneous photocatalytic systems that imply the use of an inert catalyst, non-hazardous oxidants and UV and/or visible light input. Heterogeneous photocatalysis is attracting extensive interest for the degradation of organic pollutants [6–11] and the production of self-cleaning [12,13] or anti-bacterial surfaces [14].

Up to now, great attention has been given to fine powders since high photocatalytic efficiency can be achieved by increasing the effective surface area of the materials. However, although results concerning the use of TiO_2 and ZnO nano-powders in the treatment of industrial effluents and/or volatile toxic compounds were very encouraging, these powders have mostly been used in water suspensions or in small-scale purification systems, thus limiting their practical use due to difficulties in their separation and recovery. Supporting photocatalytic materials on a steady substrate can eliminate this issue, opening a whole new range of applications. Based on such understanding, in the early 1990s, many photocatalytic semiconductors including TiO_2 and ZnO have been already prepared as thin films as well as fine powders using several deposition techniques [15–17]. Since then, many large scale deposition techniques, such as doctor blade and spray coating, have been adopted in order to produce TiO_2 coated surfaces with photocatalytic and self-cleaning properties [18–23].

* Corresponding author. Tel.: +30 2810 391917; fax: +30 2810 391951.
E-mail address: gkenanak@iesl.forth.gr (G. Kenanakis).

0926-860X/$ – see front matter © 2013 Elsevier B.V. All rights reserved.
http://dx.doi.org/10.1016/j.apcata.2013.07.040

Although TiO_2 has emerged as the most widely studied photocatalyst, ZnO is easier to grow either in the form of powder [24] or on top of various substrates [25–30] using chemical techniques that are environmental friendly and quite easy to handle. The activity of photocatalytic ZnO films can vary considerably and is dependent on many factors, such as film thickness, roughness, grain size and deposition temperature, to name but a few. A drawback, however, of ZnO is that it undergoes photocorrosion under UV light illumination, resulting in a decrease of its photocatalytic activity in aqueous media [31,32]. Meanwhile, since photocatalytic activity increases with effective surface area, a rough film surface with a high surface-to-volume ratio is beneficial. On the other hand, one-dimensional nanostructured samples offer enhanced photocatalytic efficiency due to their extremely high surface-to-volume ratio [33,34]. Thus, the successful exploitation of nanostructured ZnO thin films for use in photocatalytic applications requires the development of techniques for controlling their morphology and structural properties.

In previous work, we have demonstrated that the occurrence of a thin ZnO seed layer on Corning glass and silicon (1 0 0) substrates is crucial for obtaining *c*-axis oriented ZnO nanowires with controllable dimensions [35]. Furthermore, we have already shown that ZnO nanowires grown via aqueous solution growth at 95 °C on Corning glass substrates, which were first pre-coated by either a polycrystalline or an amorphous ZnO seed layer deposited via sol–gel at 600 or 95 °C respectively, exhibit in general very good photocatalytic activity regarding the degradation of stearic acid under UV-A light exposure [36,37].

In this work, we investigate the growth and photocatalytic activity of ZnO nanowires grown via aqueous solution growth at 95 °C on sapphire (Al_2O_3) substrates, pre-coated with a thin ZnO seed layer, which was deposited by pulsed laser deposition at various substrate temperatures, in the range of 400–700 °C. The effect of deposition temperature on the structural, optical and photocatalytic properties of the ZnO samples is thoroughly studied. It is demonstrated that (a) the pulsed laser deposited ZnO seed layers show very good photocatalytic activity regarding the degradation of stearic acid under UV-A light irradiation, varying with substrate deposition temperature and (b) the occurrence of a ZnO seed layer leads to the production of *c*-axis oriented ZnO nanowires' arrays at 95 °C, which can degrade stearic acid quite efficiently under short UV-A light exposure. The wires' diameter can be accurately tuned by varying the grain size of the seed layer, i.e., the substrate deposition temperature. The influence of nanowires' crystallinity, morphology and dimensions on their photocatalytic activity is comprehensively studied. Finally, a comparison of the structural, morphological and photocatalytic properties of the nanowires' arrays grown onto ZnO seed layers deposited by either pulsed laser deposition or sol–gel [36] is undertaken.

2. Experimental details

2.1. Deposition of ZnO seed layers and nanowires

Nanostructured ZnO thin films were grown on *c*-cut α-Al_2O_3 substrates by pulsed laser deposition (PLD). A KrF excimer laser (COMPexPro 201) of wavelength 248 nm and pulse duration 25 ns, operating at a repetition rate of 10 Hz, was used for the ablation of ZnO targets. Prior to any experiment, the deposition chamber was evacuated to 10^{-5} mbar and the substrates were in situ thermally treated at 600 °C for 30 min to remove carbon contaminants from the surface [38]. During deposition the working pressure was maintained at 0.2 mbar using high purity oxygen as background gas. The target-to-substrate distance was set at 6 cm and a fluence of ~2 J cm^{-2} was used for the ablation of ZnO target.

ZnO thin films with a thickness of 180 ± 5 nm, which were subsequently used as seed layers for the aqueous solution growth of ZnO nanowires' arrays, were deposited at 400, 500, 600 and 700 °C. The thickness of the seed layers was always kept constant (180 ± 5 nm) for every substrate temperature applied and was measured using both a non-contact optical profilometer (Ambios Technology, Xi-100) and a stylus profilometer (Alpha-step 100, Tencor).

ZnO nanowires' arrays were subsequently grown on sapphire (0 0 1) substrates, pre-coated with ZnO seed layers deposited via the PLD technique, using an equimolar (0.01 M) aqueous solution of $Zn(NO_3)_2{\cdot}6H_2O$ and $C_6H_{12}N_4$ [25,26,35,39]. In brief, laboratory Pyrex glass bottles with polypropylene autoclavable screw caps were initially filled with the solution described above. Subsequently, the substrates pre-coated with the ZnO seed layers were placed in the bottles facing downwards and heated at a constant temperature of 95 °C for 5 h in a regular laboratory oven (Memmert UNP 400). The samples were then thoroughly washed with MilliQ (18.2 MΩ cm) water to eliminate residual salts or amino complexes, and dried in air at the same temperature. Prior to deposition, all substrates used were ultrasonically cleaned with spectroscopic grade propanol and acetone, rinsed with MilliQ water and dried under N_2 gas flow.

2.2. Characterization techniques

The crystal structure of all ZnO samples was determined by X-ray diffraction (XRD) using a Rigaku (RINT 2000) diffractometer with Cu Kα (λ = 1.5406 Å) X-rays, while their surface morphology was studied by means of a field emission scanning electron microscope (FE-SEM, JEOL JSM-7000F) and an atomic force microscope (AFM) in tapping mode (Digital Instruments – Nanoscope IIIa). The surface roughness (RMS) of the ZnO thin films was determined using the scanning probe image processor (SPIP, v. 3.3.5.0) image processing software for nano- and micro-scale microscopy from Image Metrology. Finally, UV–Vis transmission spectra were recorded using a Shimadzu UV-2401 spectrophotometer over the wavelength range of 190–990 nm.

2.3. Photocatalytic activity study

Many different methods have been reported in order to determine the activity of photocatalytic surfaces. Popular techniques include those based on the photo-oxidation of organic films such as stearic acid [40–50] or palmitic acid [51,52], liquid phenolic pollutants [53,54] or organic vapors [55] and contact angle changes [56].

The photocatalytic activity of our ZnO samples was determined using stearic acid (SA) as a model compound, in which a thin layer of SA is deposited onto the film and its photocatalytic destruction is monitored as a function of time [40–50]. This method has gained preference over the years since SA provides a reasonable model compound for solid films that deposit on exterior and interior surfaces. Moreover, SA is very stable under UV illumination in the absence of a photocatalyst film (phenomenon of photolysis). Furthermore, SA can be easily laid down from a methanol or chloroform solution making the test much easier.

In order to deposit SA on the ZnO films and nanostructures, a droplet of 30 μL of a 0.1 M SA solution in chloroform was spin-coated on the sample surface under test at a rotation speed of 500 rpm for 30 s. Samples were then dried at 80 °C in air for 10 min.

The decomposition of SA can be demonstrated by FT-IR spectroscopy through the monitoring of the asymmetric C—H stretching mode of the CH_3 group at 2958 cm^{-1} and the asymmetric and symmetric C—H stretching modes of the CH_2 group at 2923 and 2853 cm^{-1}, respectively [40–50]. The photocatalytic activity experiments on all ZnO samples for the decomposition of SA were

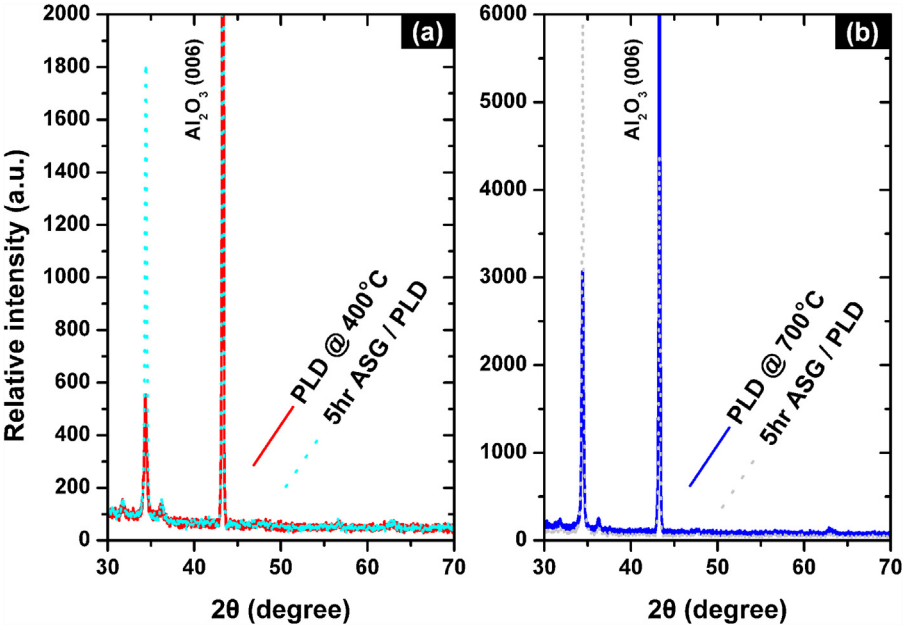

Fig. 1. XRD patterns of (a) ZnO nanowires grown by ASG for 5 h (cyan dotted curve) on sapphire substrates pre-coated with a 180 ± 5 nm thick ZnO seed layer deposited at 400 °C (red solid curve), (b) ZnO nanowires grown by ASG for 5 h (gray dotted curve) on sapphire substrates pre-coated with a 180 ± 5 nm thick ZnO seed layer deposited at 700 °C (blue solid curve). For interpretation of the references to color in this figure legend, the reader is referred to the web version of this article..

performed in ambient air and were repeated for five times demonstrating no changes in the percentage of SA conversion. The integrated area of the SA C—H stretching peaks (2800–3000 cm^{-1}) was monitored using a Fourier transform infrared spectrometer (FT-IR, IRPrestige-21, Shimadzu) before and after black light illumination in a box reactor at certain time intervals. The light source used was an HPK 125W Philips mercury lamp with main emission wavelength at 365 nm and an incident light intensity of 10 mW/cm^2. For ease in comparison of the photocatalytic activity between different samples, the integrated area of the C—H stretching peaks (2800–3000 cm^{-1}) measured at each irradiation time interval was normalized to the initial integrated area (prior to the irradiation) in order to calculate the percentage of SA remaining as a function of irradiation time. Blank experiments (photolysis) were also performed using bare sapphire (Al_2O_3) substrates under exactly the same conditions applied for the ZnO samples. Finally, the SA disappearance rate (mol/min) and the formal quantum efficiency (FQE) for all ZnO samples were calculated according to the methodology of Mills and Wang [41].

3. Results and discussions

Fig. 1(a) and (b) depict X-ray diffraction patterns of ZnO seed layers deposited by the PLD technique (solid lines) and nanowires' arrays (dashed lines) grown by aqueous solution growth (ASG) for 5 h on sapphire (0 0 1) substrates, which were initially pre-coated with ZnO seed layers deposited by PLD at 400 (Fig. 1(a)) and 700 °C (Fig. 1(b)), respectively. In all cases, XRD patterns reveal a strong (0 0 2) peak at a diffraction angle of $2\theta = 34.42°$, in good agreement with the JCPDS card (No. 36-1451) for a typical hexagonal wurtzite type ZnO crystal. Another peak at $2\theta = 43.26°$, attributed to the α-Al_2O_3 (0 0 6) reflection of sapphire, can also be detected. It can be observed that no other characteristic peaks corresponding to possible impurities, such as zinc nitrate or zinc hydroxide, are observed in the XRD patterns.

From Fig. 1 it can be also observed that the ZnO samples deposited by ASG show narrower (0 0 2) reflections with significantly higher intensity than the PLD deposited ZnO seed layers (Fig. 1(a) and (b)). The Full Width at Half Maximum (FWHM) value for the (0 0 2) peak varies from 0.360° to 0.237° for the ZnO seed layers deposited by PLD at 400 °C and 700 °C, respectively. In general, the crystallinity of the ZnO seed layers as well as their orientation along the *c*-axis increases with deposition temperature, i.e. the FWHM values for the (0 0 2) reflection are 0.360, 0.286, 0.254 and 0.237° for 400, 500, 600 and 700 °C, respectively. On the other hand, FWHM values of 0.254 and 0.225° are observed for ZnO samples grown via ASG for 5 h on sapphire substrates, which were first pre-coated with 180 ± 5 nm-thick ZnO seed layers, deposited at 400 and 700 °C by PLD, respectively. These FWHM values corresponding to the ASG samples are smaller than those observed for the ZnO seed layers deposited by PLD, indicating better crystallinity and *c*-axis growth orientation for the ASG samples. It is therefore concluded that the occurrence of a thin ZnO seed layer deposited by PLD essentially assists the growth of well-crystalline (0 0 2) oriented ZnO samples onto sapphire substrates due to the polar nature of the ZnO surface and the matching lattice structure [57], as it has been previously already reported for Corning glass substrates pre-coated with ZnO seed layers deposited via sol–gel [35–37]. It is though observed that ZnO samples grown via ASG on PLD deposited seed layers show generally less preferential growth orientation along the *c*-axis than the ones grown on seed layers prepared via the sol–gel method [35,36]. For example, the FWHM value for the (0 0 2) peak observed in the case of the ZnO sample grown via ASG for 5 h on a sapphire substrate pre-coated with a 180 nm-thick seed layer deposited by PLD at 700 °C is ~0.225°, while that of an ASG ZnO sample grown again for 5 h on a Corning glass substrate which was first pre-coated with a 140 nm-thick ZnO seed layer deposited by sol–gel at 600 °C is ~0.174° [35]. This is probably, amongst others, attributed to the poorer *c*-axis orientation of the PLD seed layers (the FWHM value for the (0 0 2) peak is ~0.237° at a deposition temperature of 700 °C) compared to the sol–gel ones (the FWHM value for the (0 0 2) peak is ~0.205° at 600 °C). An additionally important effect, which affects the preferential *c*-axis growth of ZnO samples grown via ASG, is that of the seed layer morphology and it will be discussed in the next paragraphs.

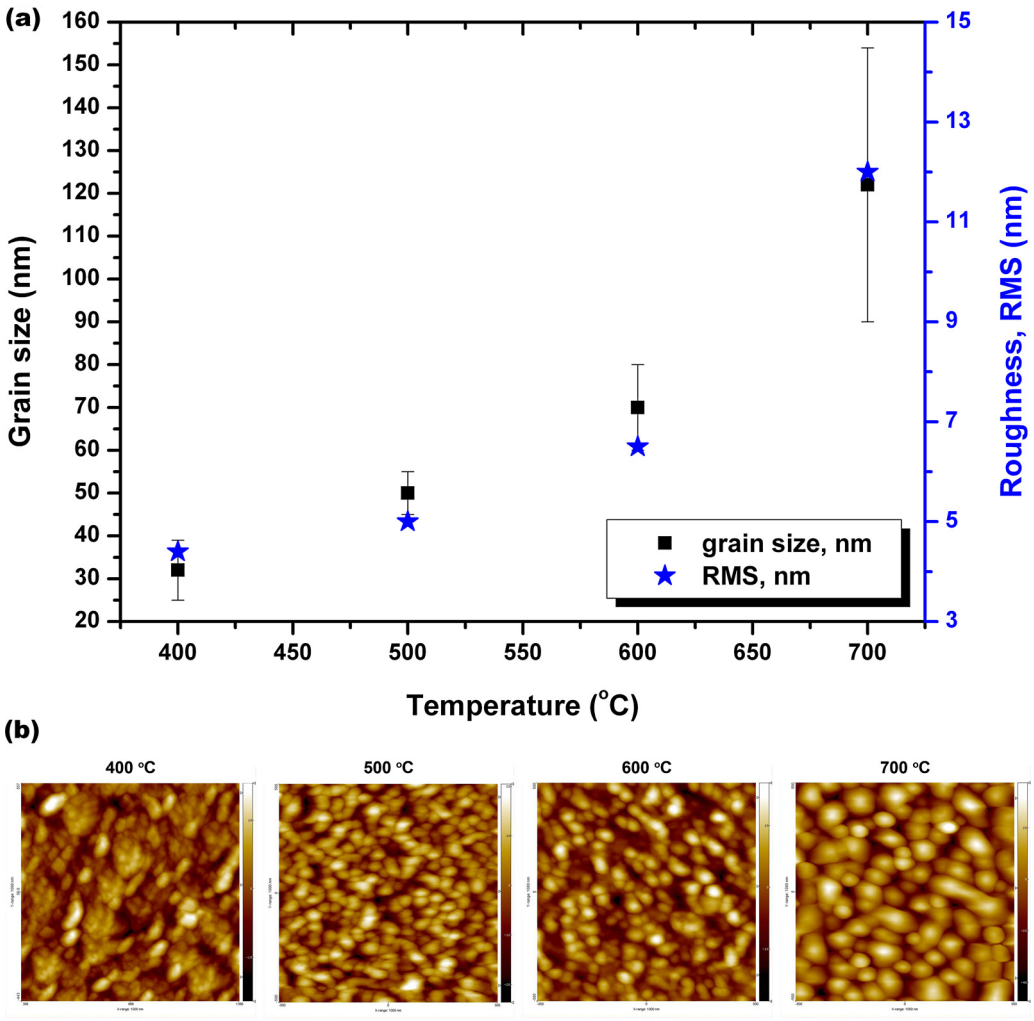

Fig. 2. (a) Grain size (black squares) and roughness (blue stars) vs. deposition temperature and (b) AFM images (scan size 1 × 1 μm) of ZnO seed layers on sapphire substrates by PLD at (left to right) 400 °C, 500 °C, 600 °C and 700 °C, respectively. For interpretation of the references to color in this figure legend, the reader is referred to the web version of this article.

Fig. 2(a) exhibits the variation of grain size and surface roughness (RMS) of the as-deposited ZnO seed layers as a function of PLD deposition temperature. The grain size, as well as the layer roughness, gradually increases with deposition temperature (see Fig. 2(a)). In particular, the ZnO seed layer deposited at 400 °C shows a grain size of ~32 ± 7 nm and a roughness of ~4 nm, while the ZnO seed layer deposited at 500 °C, has a grain size of ~50 ± 5 nm and a roughness of ~5 nm. These grain size and roughness values become even higher for the cases of 600 °C (grain size ~70 ± 10 nm, roughness ~6 nm) and 700 °C (grain size ~122 ± 32 nm, roughness ~12 nm). Moreover, one can notice from Fig. 2(b) that the ZnO seed layer deposited at 400 °C, even though it consists of the smallest grains (~32 ± 7 nm), it forms big agglomerations with a relative maximum size of ~175 ± 27 nm. This inhomogeneous morphology observed for the ZnO seed layer deposited at 400 °C could be associated with the corresponding XRD data presented in Fig. 1(a), since for this temperature (400 °C), the smallest relative intensity (~555 a.u.) along with the biggest FWHM value (0.360°) are observed for the (0 0 2) peak, indicating that the ZnO seed layer deposited at 400 °C is certainly the least crystalline sample. Hence, it can be concluded from XRD and AFM measurements that both crystallinity and *c*-axis preferred growth orientation of the ZnO seed layers increase with deposition temperature. Moreover, all ZnO seed layers deposited by PLD on sapphire substrates at 400–700 °C show significantly less homogeneity and more, as well as bigger, agglomerations, than the respective ZnO seeds grown via the sol–gel technique at 600 °C [36]. These morphology inhomogeneities are probably closely related with the reduced preferred growth orientation along the *c*-axis exhibited by the ZnO nanowires grown via ASG on sapphire substrates, which were first covered with a ZnO seed layer fabricated by PLD, compared to the ones grown on Corning glass substrates pre-coated with a ZnO seed layer deposited via sol–gel at 600 °C.

Fig. 3 displays SEM micrographs of the ZnO samples grown via ASG for 5 h on sapphire substrates, pre-coated with PLD deposited seeds with a thickness of 180 ± 5 nm at deposition temperatures ranging from 400 to 700 °C. It can be observed that in all cases nanowires' arrays are formed, with a strong *c*-axis growth orientation, i.e. perpendicular to the sapphire substrates applied. All nanowires have a hexagonal shape, in agreement with the XRD results, demonstrating the occurrence of the ZnO wurtzite crystal structure with a clear preferential growth orientation along the *c*-axis. The diameter of the ZnO nanowires gradually increases with the deposition temperature of the seed layers, ranging from ~40 ± 15 nm for 400 °C (see Fig. 3(a)) to ~155 ± 65 nm for 700 °C (Fig. 3(d)). In the case of 500 °C (Fig. 3(b)), the ZnO nanowires' diameter is ~60 ± 10 nm, while for 600 °C it reaches ~80 ± 20 nm (Fig. 3(c)). The ZnO nanowires' diameter increase with deposition temperature could be directly related to the grain size of the PLD seed layers. As it has been already mentioned, the grain

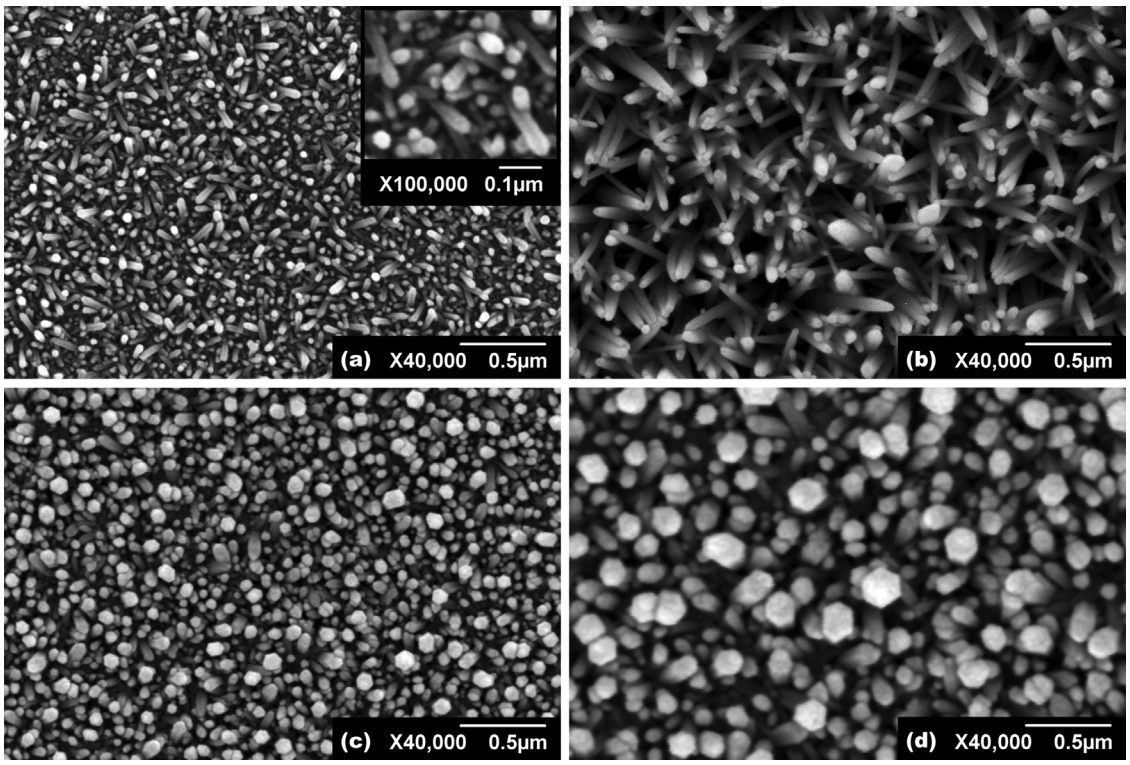

Fig. 3. SEM images (×40 000) of ZnO nanowires grown by ASG for 5 h on sapphire substrates pre-coated with a 180 ± 5 nm thick ZnO seed layer deposited by PLD at 400 °C (a), 500 °C (b), 600 °C (c) and 700 °C (d), respectively. In the inset of (a) a × 100 000 magnification of ZnO nanowires grown by ASG on a ZnO seed layer deposited by PLD at 400 °C can be observed.

size as well as the roughness of the ZnO seed layers deposited by PLD increases with deposition temperature (see Fig. 2). Specifically, the grain size values of the ZnO seed layers are ~32 ± 7 nm, ~50 ± 5 nm, ~70 ± 10 nm and ~122 ± 32 nm for 400, 500, 600 and 700 °C, respectively. As it can be readily seen, the grain size values of the seed layers are quite close to the diameter values for the corresponding ZnO nanowires' arrays. It is concluded that the presence of a ZnO seed layer fabricated by PLD leads to the formation of *c*-axis oriented ZnO nanowires via ASG onto sapphire substrates at 95 °C, and that the nanowires' diameter increases with deposition temperature, the later occurring due to a respective increase of the seed layer's grain size.

When looking though more carefully to the SEM pictures of Fig. 3(a)–(d), one can notice that the nanowires emerging are not always perfectly aligned along the *c*-axis, i.e. perpendicular to the sapphire substrates, especially for the lower deposition temperatures, namely 400 and 500 °C (Fig. 3(a) and (b)). This is attributed to the reduced *c*-axis preferred growth orientation of the corresponding seeds (the FWHM values of the (0 0 2) reflection are 0.360° and 0.286° for 400 and 500 °C, respectively) and the agglomerates formed at these temperatures. For higher deposition temperatures, i.e. 600 and 700 °C, the wires formed are much better aligned along the *c*-axis due to the increased crystallinity (the FWHM values of the (0 0 2) reflection are 0.254° and 0.237° for 600 and 700 °C, respectively) and the homogeneity of the seeds. However, it can be noticed that although the ZnO nanowires grown via ASG on PLD seeded sapphire substrates at 600 and 700 °C show very good *c*-axis growth orientation, similar to that observed for ZnO nanowires grown on sol–gel seeded Corning glass substrates at 600 °C [36], the later present smaller wire diameter deviation than the former ones. In specific, while the nanowires grown via ASG at 95 °C on sapphire substrates, which were pre-coated with a 180 nm-thick ZnO seed layer deposited by PLD at 600 °C, have a diameter of ~80 ± 20 nm, the wires grown via ASG under the same conditions onto Corning glass substrates having either a 140 nm or a 210 nm-thick ZnO seed layer on top, which was prepared by sol–gel at 600 °C, show a diameter of ~105 ± 15 nm and ~160 ± 10 nm, respectively [36].

In every case of Fig. 3(a)–(d), i.e., ZnO samples grown via ASG on sapphire substrates, which were first pre-coated with ZnO seed layers deposited by PLD at 400–700 °C, the length of the ZnO nanowires is in the range of 700–1000 nm, indicating that the only parameter that affects the nanowires' length is growth time [35]. Taking into account the wires' dimensions, i.e., their length and diameter, one can calculate the aspect ratio (L/D, length over diameter) of the ZnO nanowires. It is noticed that ZnO nanowires grown for 5 h via ASG on sapphire substrates covered with a 180 ± 5 nm-thick ZnO seed layer deposited by PLD at 400, 500, 600 and 700 °C show an aspect ratio (L/D) of 12.7–40, 10–20, 8.75–16.67 and 4.55–11.11, respectively. It is thus observed that the aspect ratio, (L/D), of the ZnO nanowires becomes higher in the cases where the PLD seeds are deposited at lower deposition temperatures, i.e., 400 and 500 °C, while it exhibits smaller values for seed layers prepared at 600 and 700 °C. This effect is directly related with the diameter of the ZnO nanowires, which increases with deposition temperature of the seed layers due to the observed increase in their grain size (see Fig. 2).

The optical transmittance spectra of the ZnO seed layers and the nanowires' arrays in the wavelength region 190–990 nm are presented in Fig. 4. As it can be seen, all transmittance spectra exhibit fringes associated with interference effects, which confirm the optical homogeneity and surface quality of the ZnO thin films deposited by PLD. Both ZnO seed layers and nanowires' arrays are quite transparent in the visible regime and exhibit a sharp absorption band in the UV region that can be attributed to excitonic resonances [58]. Regarding the optical energy gap of the samples, E_{gap}, this was determined using "Tauc" plots [59] of α^2 as a function of $h\nu$ and found to be 3.258, 3.260, 3.267 and 3.280 eV for the ZnO seed layers deposited at 400, 500, 600 and 700 °C, respectively, values

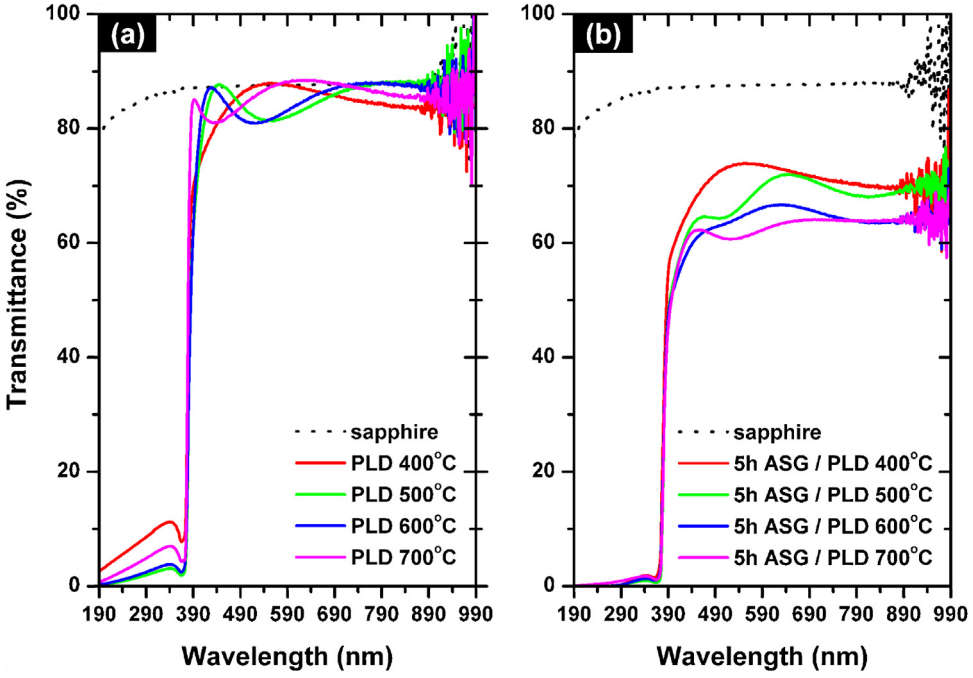

Fig. 4. Optical transmittance spectra of (a) 180 ± 5 nm thick ZnO seed layers deposited by PLD on sapphire substrates at 400 °C, 500 °C, 600 °C and 700 °C, respectively, and (b) ZnO nanowires grown by ASG for 5 h on ZnO seed layers deposited by PLD on sapphire substrates at 400 °C, 500 °C, 600 °C and 700 °C, respectively.

similar to the ones reported in the literature for high quality ZnO films deposited using the PLD technique [60,61]. As it can be seen, the E_{gap} of the ZnO seed layers gradually increases with deposition temperature, most probably due to the corresponding increase in their grain size (see Fig. 2). The E_{gap} values were also estimated for the ZnO nanowires' arrays grown on seeded sapphire substrates via ASG and found to be in the range of 3.203–3.247 eV, in agreement with values reported earlier by other research groups using aqueous solution approaches [62–64]. This change in E_{gap} is mostly attributed to the different size and morphologies of the as-grown ZnO nanowires [62].

Furthermore, it can be noticed that the transmittance of the ZnO seed layers varies from 82.4 to 88.4% at 600 nm depending on deposition temperature, while for the ASG samples it lies between 62.6 and 73.6%. This reduction in transmittance can most probably be attributed to the thickness increase observed for the ASG samples. However, the chemically grown ZnO nanowires still exhibit relatively high transmittance values, especially the ones grown on sapphire substrates pre-coated with seed layers deposited by PLD at 400 and 500 °C, namely 73.6 and 70.7%, respectively.

Fig. 5(a) displays the normalized integrated area vs. irradiation time curves for the ZnO seed layers fabricated by PLD at various deposition temperatures. It can be noticed that the seed layer deposited at 400 °C shows poor photocatalytic activity since it degrades SA by only 52% at 30 min. However, SA conversion reaches ~79% at 120 min. When the deposition temperature rises up to 500 °C, the conversion of SA at 30 min reaches 92.5%. This remarkable photocatalytic activity increase is due to much better crystallinity and *c*-axis preferred growth orientation of the ZnO seed layer deposited at 500 °C compared to 400 °C. As the deposition temperature further increases to 600 °C, the photocatalytic activity of the ZnO seed layer at 30 min reduces to ~76%, still reaching ~97% at 120 min. The reduction in the photocatalytic activity after 30 min UV-A irradiation for the ZnO seed layer deposited at 600 °C is most probably attributed to the observed increase in grain size compared to 500 °C, i.e., it exhibits a grain size value of ~70 ± 10 nm instead of ~50 ± 5 nm for 500 °C (see Fig. 2). Specifically, the grain size increase leads to smaller surface area and thus minor photocatalytic activity. At the same time the crystallinity and *c*-axis growth orientation of the ZnO seed layer deposited at 600 °C are comparable to those observed for 500 °C, i.e., the FWHM values for the (0 0 2) peak are 0.286 and 0.254° for 500 and 600 °C, respectively. Finally, when the deposition temperature increases to 700 °C, the photocatalytic activity of the ZnO seed layer rapidly drops to ~32% at 30 min and hardly reaches ~77% after irradiation for 120 min. The rather reduced photocatalytic activity observed for 700 °C is mainly because of the quite larger grain size (~122 ± 32 nm) that this seed layer exhibits compared to samples deposited at lower deposition temperatures, while, at the same time, its crystallinity and *c*-axis preferred growth orientation are similar to 500 and 600 °C. However, for all deposition temperatures, even for 700 °C, the photocatalytic activity of the ZnO seed layers regarding the percentage of conversion of SA is always significantly higher than that observed due to photolysis, i.e., light irradiation of SA in the absence of a metal oxide catalyst. At 30 min, for example, the percentage of SA conversion due to photolysis is only ~8%, reaching barely 31% after 120 min of irradiation, as a result of a decrease of the asymmetric and symmetric C—H stretching modes of the CH_2 group at 2923 and 2853 cm^{-1} respectively.

In Fig. 5(b), the photocatalytic activity results in terms of percentage of SA conversion are presented for the ZnO nanowires' arrays grown via ASG at 95 °C on sapphire substrates, which were first pre-coated with ZnO seed layers deposited by PLD at 400, 500, 600 and 700 °C. It can be readily seen that all samples show remarkable photocatalytic activity, degrading SA by more than 73% at 120 min. The respective percentage of conversion of SA due to photolysis is only 31%, much smaller than that of all ASG samples grown on ZnO seed layers deposited by PLD. It can be seen that the photocatalytic activity of the chemically grown ZnO nanowires' arrays at first increases with the substrate deposition temperature of the seed layers. The percentage of SA conversion at 30 min takes values of 52, 64 and 85% for 400, 500 and 600 °C, respectively. It subsequently reaches 84, 91 and ~100% at 120 min. The increase in the photocatalytic activity of the ASG samples with deposition temperature is most probably due to better crystallinity, enhanced alignment of the ZnO nanowires along the *c*-axis, i.e., perpendicular

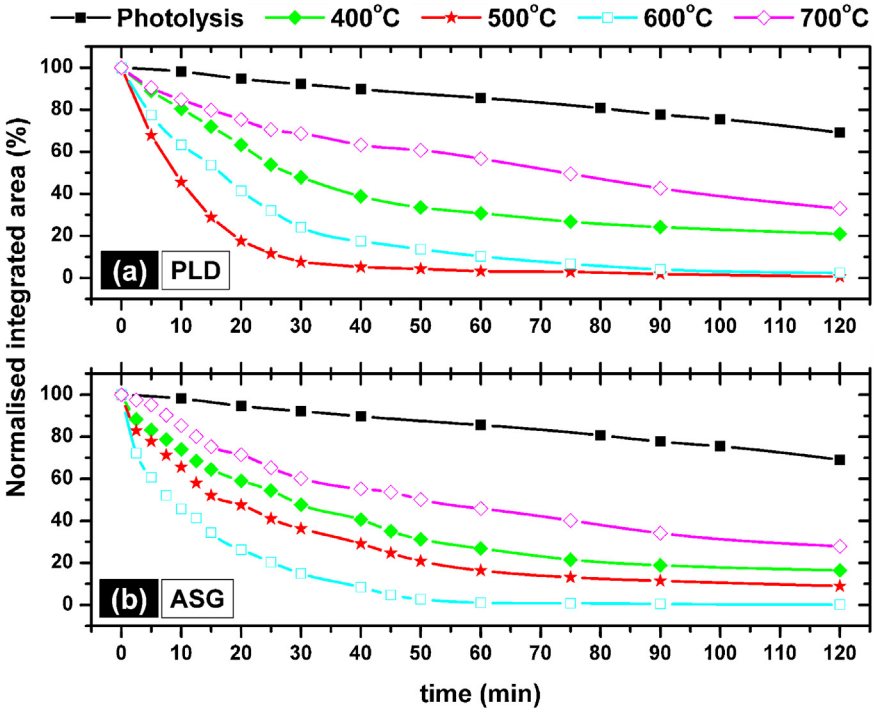

Fig. 5. Normalized integrated area vs. irradiation time for (a) 180 ± 5 nm thick ZnO seed layers deposited by PLD on sapphire substrates at 400 °C (solid green rhombuses), 500 °C (red stars), 600 °C (open cyan squares) and 700 °C (open magenta rhombuses) and (b) ZnO nanowires grown at 95 °C by ASG on sapphire substrates pre-coated with 180 ± 5 nm thick ZnO seed layers, which were deposited by PLD at 400 °C (solid green rhombuses), 500 °C (red stars), 600 °C (open cyan squares) and 700 °C (open magenta rhombuses). For comparison, the photolysis curve (black solid squares) is also presented. For interpretation of the references to color in this figure legend, the reader is referred to the web version of this article.

to the substrate applied, improved morphology homogeneity (see Fig. 3(a)–(c)), together with increased UV absorbance (see Fig. 4). On the other hand, the nanowires' aspect ratio (L/D), which gradually decreases with increasing deposition temperature, i.e., it takes values of 12.7–40, 10–20, 8.75–16.67 for 400, 500 and 600 °C respectively, does not seem to affect the photocatalytic activity of the ASG samples as much as the nanowires' crystallinity, *c*-axis alignment and morphological homogeneity. When the deposition temperature of the ZnO seed layer, however, increases to 700 °C, the photocatalytic activity of the solution grown nanowires' array dramatically drops to 40% at 30 min, reaching hardly 73% at 120 min. This photocatalytic activity drop observed for 700 °C could be mainly attributed to the abrupt decrease of the aspect ratio (L/D) of the ZnO nanowires' array. In particular (L/D) falls down to 4.55–11.11 for 700 °C, signifying a rapid decrease in the sample's surface area compared with the ASG samples grown at $T \leq 600$ °C. This large surface area decrease cannot be apparently outbalanced from the increase in crystallinity and *c*-axis preferred growth orientation at 700 °C (FWHM values for the (0 0 2) reflection are 0.254 and 0.225° for 400 and 700 °C, respectively), as well as the nanowires' morphology homogeneity (see Fig. 3(a)–(d)), and in turn leads to the observed photocatalytic activity considerable drop for 700 °C.

It can also be observed that the photocatalytic activity of the ZnO nanowires' arrays is generally comparable with that of the seed layers, showing similar percentage of SA conversion both at 30 and 120 min. For example, the ZnO seed layer deposited by PLD at 400 °C exhibits percentage of SA destruction values of 52 and 79%, respectively, while the ZnO nanowires' array grown via ASG on top of it shows corresponding percentage of SA conversion values of 52 and 84% (see Fig. 5(a) and (b)). The photocatalytic activity at 30 min for all pulsed laser deposited ZnO seed layers and chemically grown nanowires is summarized in Table 1, where the SA disappearance rate (mol/min) and the formal quantum efficiency (FQE) are also presented [41]. It can be noticed that the ZnO nanowires' array grown via ASG on top of a seed layer deposited by PLD at 600 °C shows the highest SA disappearance rate and FQE at 30 min, i.e., 4.22×10^{-8} mol/min and 4.48×10^{-3} respectively.

Finally, the percentage of SA conversion values displayed at 30 min for the PLD deposited seeds (180 nm-thick) and the corresponding ASG ZnO nanowires' arrays are comparable to the ones observed previously for nanowires' arrays grown via ASG on Corning glass substrates covered with ZnO seed layers (140 and 210 nm-thick), which were fabricated by sol–gel [36]. Specifically, in the case of ASG ZnO samples grown for 5 h onto Corning glass substrates, pre-coated with a 140 or 210 nm-thick seed layer deposited by sol–gel at 600 °C, the percentage of SA destruction at 30 min was reported to be 81 and 58%, respectively [36]. At the same time, the percentage of SA conversion for the ASG ZnO sample

Table 1
Photocatalytic activity at 30 min, initial stearic acid disappearance rate (mol/min) and formal quantum efficiency (FQE, see Mills and Wang [41]) for all ZnO seed layers and chemically grown nanowires' arrays.

	Photolysis	400 °C	5 h ASG/400 °C	500 °C	5 h ASG/500 °C	600 °C	5 h ASG/600 °C	700 °C	5 h ASG/700 °C
α (%) at 30 min	7.85%	52.21%	52.31%	92.45%	63.76%	75.94%	85.03%	31.37%	39.82%
Initial SA disappearance rate (mol/min)	4.44×10^{-10}	9.07×10^{-9}	1.80×10^{-8}	2.56×10^{-8}	2.38×10^{-8}	1.68×10^{-8}	4.22×10^{-8}	7.09×10^{-9}	5.22×10^{-9}
Formal Quantum Efficiency, $(FQE)_{(SA)}/10^{-3}$	0.05	0.96	1.91	2.71	2.53	1.78	4.48	0.75	0.55

grown on a sapphire substrate pre-coated with a 180 nm-thick seed layer deposited by PLD at 600 °C is 85% (Fig. 5(b)).

4. Conclusions

ZnO nanowires' arrays were grown at 95 °C for 5 h onto sapphire substrates, which were pre-coated with a ZnO seed layer deposited by the PLD technique at various substrate temperatures, namely 400, 500, 600 and 700 °C. In general, the crystallinity of the ZnO seed layers as well as their orientation along the *c*-axis increases with deposition temperature. The chemically grown ZnO nanowires show narrower (0 0 2) reflections with significantly higher intensity than the seed layers deposited by PLD. The grain size, as well as the seed layer roughness, gradually increases with substrate deposition temperature. At the same time, the diameter of the ZnO nanowires increases with seed layer's deposition temperature, ranging from ~40 ± 15 nm for 400 °C to ~155 ± 65 nm for 700 °C, respectively. This increase in the wires' diameter is directly related to the corresponding increase of the seed layer's grain size with deposition temperature. For higher deposition temperatures, i.e. 600 and 700 °C, the ZnO nanowires formed are much better aligned along the *c*-axis due to the increased crystallinity and homogeneity of the seed layers. On the other hand, the length of all ZnO nanowires' arrays lies in the range of 700–1000 nm, indicating that the only parameter that affects the nanowires' length is growth time. Both ZnO seed layers and nanowires' arrays are quite transparent in the visible regime. The E_{gap} of the ZnO seed layers gradually increases with deposition temperature, most probably due to the corresponding increase in their grain size. The chemically grown ZnO nanowires exhibit relatively high transmittance values, especially the ones grown on sapphire substrates pre-coated with seed layers deposited by PLD at 400 and 500 °C, namely 73.6 and 70.7%, respectively. All ZnO samples, including seed layers and nanowires' arrays, show very good photocatalytic activity regarding the degradation of stearic acid under UV-A light exposure. Among the seed layers deposited by PLD, the one fabricated at 500 °C shows the best photocatalytic activity, degrading SA by 92.5% at 30 min (FQE = 2.71×10^{-3}). This is due to its very good crystallinity, *c*-axis preferred growth orientation and small grain size (~50 ± 5 nm), i.e., large surface area. When the deposition temperature increases, the photocatalytic activity of the ZnO seed layers drops, the percentage of SA conversion for 700 °C reaches hardly ~32% at 30 min (FQE = 0.75×10^{-3}), due to quite larger grain size (~122 ± 32 nm for 700 °C). In addition, the photocatalytic activity of the ZnO nanowires' arrays is quite remarkable, the percentage of SA conversion reaching 85% (FQE = 4.48×10^{-3}) and ~100% at 30 and 120 min, respectively, for the sample which was chemically grown on top of a ZnO seed layer deposited by PLD at 600 °C. The photocatalytic activity drop observed for 700 °C is mainly attributed to the abrupt decrease of the aspect ratio (L/D) of the ZnO nanowires' array, i.e., (L/D) falls down to 4.55–11.11. It is finally concluded that the application of the ASG technique at 95 °C on sapphire substrates, pre-coated with ZnO seed layers deposited by PLD, leads to one-dimensional ZnO nanostructures with enhanced photocatalytic activity, which is mainly controlled by their surface-to-volume ratio (i.e., aspect ratio of the nanowires' arrays, (L/D)), crystallinity, nanowires' *c*-axis alignment, morphology homogeneity and light absorbance.

Acknowledgements

This project is implemented through the Operational Programme "Education and Lifelong Learning", Action Archimedes III and is co-financed by the European Union (European Social Fund) and Greek national funds (National Strategic Reference Framework 2007–2013).

References

[1] K. Hashimoto, H. Irie, A. Fujishima, Jpn. J. Appl. Phys. 44 (2005) 8269–8285.
[2] S. Kansal, M. Singh, D. Sud, J. Hazard. Mater. 141 (2007) 581–590.
[3] M. Stylidi, D. Kontarides, X. Verykios, Appl. Catal. B 40 (2003) 271–286.
[4] A. Houas, H. Lachheb, M. Ksibi, E. Elaloui, C. Guillard, J. Herrmann, Appl. Catal. B 31 (2001) 145–157.
[5] H. Lachheb, E. Puzenat, A. Houas, M. Ksibi, E. Elaloui, C. Guillard, J.M. Herrmann, Appl. Catal. B 39 (2002) 75–90.
[6] A. Mills, S. Lee, J. Photochem. Photobiol. A 152 (2002) 233–247.
[7] I.M. Arabatzis, S. Antonaraki, T. Stergiopoulos, A. Hiskia, E. Papaconstantinou, M.C. Bernard, P. Falaras, J. Photochem. Photobiol. A 149 (2002) 237–245.
[8] S.B. Kim, S.C. Hong, Appl. Catal. 35 (2002) 305–315.
[9] Y.H. Hsien, C.F. Chang, Y.H. Chen, S.F. Chang, Appl. Catal. B 31 (2001) 241–249.
[10] M. Pelaez, N.T. Nolan, S.C. Pillai, M.K. Seery, P. Falaras, A.G. Kontos, P.S.M. Dunlop, J.W.J. Hamilton, J.A. Byrne, K. O'Shea, M.H. Enterazi, D.D. Dionysiou, Appl. Catal. B 125 (2012) 331–349.
[11] L. Xiao-e, A.N.M. Green, S.A. Haque, A. Mills, J.R. Durrant, J. Photochem. Photobiol. A 162 (2004) 253–259.
[12] K. Guan, Surf. Coat. Technol. 191 (2005) 155–160.
[13] G. Kenanakis, E. Stratakis, K. Vlachou, D. Vernardou, E. Koudoumas, N. Katsarakis, Appl. Surf. Sci. 254 (2008) 5695–5699.
[14] S.H. Lee, S. Pumprueg, B. Moudgil, W. Sigmund, Colloid Surf. B 40 (2005) 93–98.
[15] A. Mills, S. Le Hunte, J. Photochem. Photobiol. A 108 (1997) 1–35.
[16] M. Suzuki, T. Ito, Y. Taga, Appl. Phys. Lett. 78 (2001) 3968–3970.
[17] P.V. Kamat, R. Huehn, R. Nicolaescu, J. Phys. Chem. B 106 (2002) 788–794.
[18] L. Lopez, W.A. Daoud, D. Dutta, Surf. Coat. Technol. 2 (15) (2010) 251–257.
[19] R. Wang, K. Hashimoto, A. Fujishima, M. Chikuni, E. Kojima, A. Kitamura, M. Shimohigoshi, T. Watanabe, Adv. Mater. 10 (2) (1998) 135–138.
[20] A. Fujishima, X. Zhang, C. R. Chim. 9 (2006) 750–760.
[21] A. Fujishima, X. Zhang, D.A. Tryk, Surf. Sci. Rep. 63 (2008) 515–582.
[22] M.A. Henderson, Surf. Sci. Rep. 66 (2011) 185–297.
[23] T. Bak, T. Norby, J. Nowotny, N.K. Nowotny, N. Sucher, Solid State Phenom. 162 (2010) 77–90.
[24] K.M. Parida, S.S. Dash, D.P. Das, J. Colloid Interface Sci. 298 (2006) 787–793.
[25] M. Andrés Vergés, M. Martinez, E. Matijević, J. Mater. Res. 8 (1993) 2916–2920.
[26] L. Vayssieres, Adv. Mater. 15 (2003) 464–466.
[27] Z. Zhang, H. Yu, Y. Wang, M.Y. Han, Nanotechnology 17 (2006) 2994–2997.
[28] J. Chen, C. Li, J.L. Song, X.W. Sun, W. Lei, W.Q. Deng, App. Surf. Sci. 255 (2009) 7508–7511.
[29] X. Hu, Y. Masuda, T. Ohji, K. Kato, J. Am. Ceram. Soc. 92 (4) (2009) 922–926.
[30] J.L. Yang, S.J. An, W.I. Park, G.C. Yi, W. Choi, Adv. Mater. 14 (16) (2004) 1661–1664.
[31] C.C. Hariharan, Appl. Catal. A: Gen. 304 (2006) 55–61.
[32] P. Spathis, I. Poulios, Corros. Sci. 37 (1995) 673–680.
[33] R. Hong, T. Pan, J. Qian, H. Li, Chem. Eng. J. 119 (2006) 71–81.
[34] L. Jing, Z. Xu, X. Sun, J. Shang, W. Cai, Appl. Surf. Sci. 180 (2001) 308–314.
[35] G. Kenanakis, D. Vernardou, E. Koudoumas, N. Katsarakis, J. Cryst. Growth 311 (2009) 4799–4804.
[36] G. Kenanakis, N. Katsarakis, Appl. Catal. A 378 (2010) 227–233.
[37] G. Kenanakis, D. Vernardou, N. Katsarakis, Appl. Catal. A 411–412 (2012) 7–14.
[38] Y. Zhao, Y. Jiang, Y. Fang, J. Cryst. Growth 307 (2007) 278–282.
[39] G. Kenanakis, D. Vernardou, E. Koudoumas, G. Kiriakidis, N. Katsarakis, Sens. Actuators B: Chem. 124 (2007) 187–191.
[40] A. Mills, S. Lee, A. Lepre, I.P. Parkin, S.A. O'Neill, Photochem. Photobiol. Sci. 1 (11) (2002) 865–868.
[41] A. Mills, J. Wang, Photochem. Photobiol. A 182 (2006) 181–186.
[42] T. Sawunyama, L. Jiang, A. Fujishima, K. Hashimoto, J. Phys. Chem. B 101 (1997) 11000–11003.
[43] M.E. Simonsen, H. Jensen, Z. Li, E.G. Søgaard, Photochem. Photobiol. A 200 (2008) 192–200.
[44] D. Vernardou, G. Kalogerakis, E. Stratakis, G. Kenanakis, E. Koudoumas, N. Katsarakis, Solid State Sci. 11 (2009) 1499–1582.
[45] D. Vernardou, E. Stratakis, G. Kenanakis, H.M. Yates, S. Couris, M.E. Pemble, E. Koudoumas, N. Katsarakis, J. Photochem. Photobiol. A 202 (2009) 81–85.
[46] G. Kenanakis, Z. Giannakoudakis, D. Vernardou, C. Savvakis, N. Katsarakis, Catal. Today 151 (2010) 34–38.
[47] Y. Paz, Z. Luo, L. Rabenberg, A. Heller, J. Mater. Res. 10 (1995) 2842–2848.
[48] N.P. Mellott, C. Durucan, C.G. Pantano, M. Guglielmi, Thin Solid Films 502 (2006) 112–120.
[49] Q. Xu, D.V. Wellia, M.A. Sk, K.H. Lim, J.S.C. Loo, D.W. Liao, R. Amal, T.T.Y. Tan, J. Photochem. Photobiol. A: Chem. 210 (2010) 181–187.
[50] L.K. Tan, M.K. Kumar, W.W. An, H. Gao, ACS Appl. Mater. Interfaces 2 (2010) 498–503.
[51] V. Romeas, P. Pichat, C. Guillard, T. Chopin, C. Lehaut, New J. Chem. 23 (1999) 365–373.
[52] J. Kasanen, M. Suvanto, T.T. Pakkanen, J. Appl. Polym. Sci. 111 (2009) 2597–2606.
[53] D. Chen, A.K. Ray, Appl. Catal. B 23 (1999) 143–157.
[54] K.M. Parida, S. Parija, Sol. Energy 80 (2006) 1048–1054.
[55] J. Shang, W. Li, Y. Zhu, J. Mol. Catal. A: Chem. 202 (2003) 187–195.

[56] A. Mills, N. Elliott, I.P. Parkin, S.A. O'Neill, R.J. Clark, J. Photochem. Photobiol. A: Chem. 151 (2002) 171–179.
[57] Z.L. Wang, Mater. Today 7 (2004) 26–33.
[58] J.A. Sans, A. Segura, M. Mollar, B. Mari, Thin Solid Films 453 (2004) 251–255.
[59] J. Tauc, in: F. Abeles (Ed.), Optical Properties of Solids, Amsterdam, North-Holland, 1972, p. 277.
[60] L. Zhao, J. Lian, Y. Liu, Q. Jiang, Appl. Surf. Sci. 252 (2006) 8451–8455.
[61] M. Suchea, S. Christoulakis, M. Katharakis, G. Kiriakidis, N. Katsarakis, E. Koudoumas, Appl. Surf. Sci. 253 (2007) 8141–8145.
[62] N. Samaele, P. Amornpitoksuk, S. Suwanboon, Powder Technol. 203 (2010) 243–247.
[63] S.A. Vanalakar, S.S. Mali, R.C. Pawar, D.S. Dalavi, A.V. Mohalkar, H.P. Deshamukh, P.S. Patil, Ceramics 38 (2012) 6461–6467.
[64] R.C. Pawar, J.S. Shaikh, A.A. Babar, P.M. Dhere, P.S. Patil, Sol. Energy 85 (2011) 1119–1127.